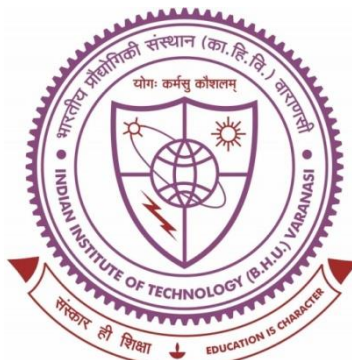


MULTIFUNCTIONAL BEHAVIOR OF FERRITE BASED PEROVSKITES FOR ENERGY APPLICATIONS



THESIS SUBMITTED IN PARTIAL FULFILLMENT FOR THE AWARD OF DEGREE

Doctor of Philosophy

In

Physics

by

UMA SHARMA

UNDER THE SUPERVISION OF

PROF. PRABHAKAR SINGH

DEPARTMENT OF PHYSICS

INDIAN INSTITUTE OF TECHNOLOGY

(BANARAS HINDU UNIVERSITY)

VARANASI – 221005

18171010

2024

CERTIFICATE

It is certified that the work contained in the thesis titled “**Multifunctional behavior of Ferrite based Perovskites for Energy Applications**” by “**UMA SHARMA**” (Roll No. **18171010**), in partial fulfillment of the requirement for the award of degree of **Doctor of Philosophy** at **Indian Institute of Technology (B.H.U), Varanasi** is a record of her own work carried out under my supervision and guidance, and this work has not been submitted elsewhere for a degree.

It is further certified that the student has fulfilled all the requirements of Comprehensive Examination, Candidacy, and SOTA for the award of Ph.D. Degree.

Date: 09/04/2024

Place: Varanasi



Supervisor

(Prof. Prabhakar Singh)

Dr. Prabhakar Singh

प्रध्याय/Professor

भौतिकी विभाग/Deptt. of Physics

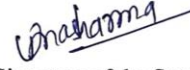
भारतीय प्रौद्योगिकी संस्थान (काठिण्डविण्ड)/ IIT (BHU)
वाराणसी/Varanasi-221005

DECLARATION BY THE CANDIDATE

I, **UMA SHARMA** (Roll No. **18171010**), certify that the work embodied in this thesis is my own bonafide work and carried out by me under the supervision of **PROF. PRABHAKAR SINGH** from **JULY, 2018** to **APRIL, 2024** at the **DEPARTMENT OF PHYSICS**, Indian Institute of Technology, Varanasi. The matter embodied in this thesis has not been submitted for the award of any other degree/diploma. I declare that I have faithfully acknowledged and given credits to the research workers wherever their works have been cited in my work in this thesis. I further declare that I have not willfully copied from any other's work, paragraphs, text, data, results, etc., reported in journals, books, magazines, reports dissertations, theses, etc., or available at websites and have not included them in this thesis and have not cited as my own work.

Date: 09/04/2024

Place: Varanasi



Signature of the Student

(UMA SHARMA)

CERTIFICATE BY THE SUPERVISOR

It is certified that the above statement made by the student is correct to the best of our knowledge.




09/04/2024
Supervisor

(Prof. Prabhakar Singh)

Dr. Prabhakar Singh

प्रभार्य/Professor

भौतिकी विभाग/Deptt. of Physics
भा०प्रौ०सं०(का०हि०वि०)/IIT (BHU)
वाराणसी/Varanasi-221005



09/04/24
Signature of Head of Department
HEAD/विभागाध्यक्ष
भौतिकी विभाग/Deptt. of Physics
भा०प्रौ०सं०(का०हि०वि०)/IIT (BHU)
वाराणसी/Varanasi-221005

COPYRIGHT TRANSFER CERTIFICATE

Title of the Thesis: "Multifunctional behavior of Ferrite based Perovskites for Energy Applications"

Name of the Student: Uma Sharma

Copyright Transfer

The undersigned hereby assigns to the Indian Institute of Technology (Banaras Hindu University) Varanasi all rights under copyright that may exist in and for the above thesis submitted for the award of the "*Doctor of Philosophy*".

Date: 09/04/2024

Place: IIT (BHU), Varanasi


Signature of the Student

(UMA SHARMA)

Note: However, the author may reproduce or authorize others to reproduce material extracted verbatim from the thesis or derivative of the thesis for author's personal use provided that the source and the Institute's copyright notice are indicated.

Acknowledgements

The doctoral journey has been a life-enriching and transformative experience. Over the past five year traveling through the ocean of knowledge, I finally got the chance to appreciate the beauty of discovering and understanding the unknown, even if lost and struggling in the mist often happened at the beginning. It would never happened without the unwavering support and help from people around me. Here, I would like to express my sincerest gratitude to all who have supported and helped me during my Ph.D. studies.

*First, I would like to express my sincere gratitude to my esteemed supervisor, **Prof. Prabhakar Singh**, for his enthusiastic encouragement, guidance, invaluable support and constructive advice throughout my doctoral studies. His indomitable zeal and diligence inspired me to bring some discipline to my own work, enabling me to systematically focus my energy towards fulfilling my goals. I am deeply thankful to him for his continuous support.*

I would like to express my sincere thanks to my research progress evaluation committee (RPEC) members, Dr. Sunil K Singh, and Dr. Ashushtosh K Dubey, for their valuable time and insightful suggestions during the entire course of this research. I offer my special thanks to Prof. Sandip Chatterjee, Head of the Department of Physics, for extending experimental facilities during this research work.

I wish to express deep regards to all the Professors of the Department for their kind support during the progress of my research.

With deep gratitude, I express my sincere appreciation to CIFC, IIT (BHU), Varanasi for their assistance in characterization of the synthesized samples. I am also thankful to all the office staff of the Department and authorities of IIT (BHU) for their kind help during my tenure, which facilitated the completion of my thesis work.

I would like to thank Dr. Pardeep K. Jha and Dr. Priyanka A. Jha, Department of Physics, IIT (BHU), Varanasi, for their invaluable suggestions and scientific views during my research work.

I would also like to thank all my senior research members Dr. Raghvendra Pandey, Dr. Vani Pawar, Dr. Pragati Singh, Dr. Vandana Tomar, Dr. Manish Kumar, Dr. Ajay Bangwal, Dr. Manisha Chauhan, Dr. Ashish Kumar Yadav, and labmates, Mr. Prem Chandra Bharti, Mr. Ashish Kumar Ranjan, Ms. Swarnima Singh, Ms. Manisha Sharma, Mr. Jaynarayan Mishra, Ms. Kamana Mishra, Mr. Vishal Singh, Mr. Hemant Kumar, Mr. Shivam Pandey, Mr. Akash Patel and all research colleagues of Department of Physics, IIT(BHU), for sharing their knowledge and creating enjoyable lab atmosphere both on and off the slopes.

The moral support and constant motivation that I have consistently received from my friends are beyond words, and I consider myself fortunate to be blessed with such amazing friends. Among them, I owe special thanks to Mr. Nikhil Kumar, Mr. Deepak Kumar Gond, Mr. Prashant Kumar Pandey, Ms. Sarika Mishra, Ms. Shambhavi Dixit, Mr. Pushpendra Kumar Yadav, Ms. Srishti Dixit, Mrs. Poornima Singh, and Dr. Neha Trivedi.

I wish to extend my heartfelt gratitude to my family, especially my parents, Shri Jagdish Prasad and Smt. Jayanti Devi, for their unwavering support, limitless love, and blessings. I am truly grateful to my elder sisters Mrs. Sadhana and Mrs. Vandana for being simply there to share laughter and joy. Reaching this point in my life would have been challenging without their support. This journey would not have been possible without these little ones: my younger sister, Ms. Ranjana Sharma, and my niece and nephews, Ms. Avika Sharma, Mr. Aryan Sharma, and Mr. Ishan Sharma. You all have been my source of comfort throughout this journey. I hope this thesis will make my family proud and bring a broader smile.

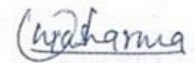
I also thank to all those who could not find a separate mention but have helped me directly or indirectly in completing this monumental task.

Last but not least, I appreciate my unwavering determination in every circumstances, steadfast self-belief, and consistency in being true to myself.

Finally, I bow with reverence and gratitude to thank the Lord Shiva for constantly showering blessings on me.

Date: 09/04/2024

Place: Varanasi



Uma Sharma

Contents

CERTIFICATE	i
DECLARATION BY THE CANDIDATE	iii
COPYRIGHT TRANSFER CERTIFICATE	v
Acknowledgements.....	vii
Contents.....	x
LIST OF FIGURES.....	xvii
LIST OF TABLES.....	xxvii
LIST OF SYMBOLS AND ABBREVIATIONS.....	xxix
PREFACE	1
CHAPTER 1: Introduction and Literature Review	1
1.1 Present Energy Scenario.....	1
1.2 Alternative Solutions	5
1.2.1 Fuel Cells.....	6
1.2.1.1 Fuel Cell Components	8
1.2.2 Batteries.....	11
1.2.3 Water Splitting	13
1.3 Importance of Electrochemical Reaction	15
1.3.1 Catalysts	16
1.3.2 Reaction Kinetics and Mechanism	17
1.3.3 Bifunctional/Multifunctional Catalysts	22
1.4 Perovskites for Energy Application.....	25
1.4.1 Perovskite Oxide	25
1.5 Background For Proposed Work (Motivation).....	36
1.5.1 Why Fe-based Perovskites?.....	36
1.5.2 Lanthanum-Doped Fe-based perovskites (La-FeO ₃).....	40

1.6	Overview of Lanthanum Ferrite (LaFeO ₃)	43
1.7	Motivation and Concluding Remarks.....	45
1.8	Objective of the Present Research Work.....	46
	CHAPTER 2: Synthesis, Characterizations, and Analysis Techniques	48
2.1	Overview	48
2.1.1	Specification of Raw Materials used.....	49
2.2	Materials Synthesis.....	49
2.2.1	Solid-State Reaction Route (SSR).....	50
2.2.2	Hydrothermal synthesis route.....	51
2.2.3	Pulse Laser Deposition Technique (PLD).....	52
2.3	Characterization Techniques	54
2.3.1	Thermal Analysis (TGA-DSC).....	54
2.3.2	X-Ray Diffraction Analysis (XRD).....	55
2.3.3	Fourier Transform Infrared Spectroscopy (FTIR).....	58
2.3.4	X-Ray Photoelectron Spectroscopy (XPS).....	59
2.3.5	Scanning Electron Microscopy (SEM).....	60
2.3.6	Ultra – Violet Visible (UV-Vis) Spectroscopy.....	62
2.3.7	Transmission Electron Microscopy (TEM).....	64
2.3.8	Atomic Force Microscopy (AFM).....	65
2.3.9	Density Measurement.....	67
2.4	Electrical Data Analysis	68
2.4.1	Conductivity Spectra	68
2.4.2	Impedance Spectroscopy Analysis	71
2.5	Electrochemical Techniques.....	75
2.5.1	Electrode preparation.....	75
2.5.2	Cyclic Voltammetry (CV)	76
2.5.3	Linear Sweep Voltammetry (LSV).....	77

2.5.4	Tafel Plot	78
2.5.5	Stability Test.....	79
2.6	Analysis Techniques.....	80
2.6.1	Rietveld Refinement Technique	80
2.6.2	Process of Analyzing the Obtained Data.....	81
CHAPTER 3: Electrochemical properties of LaFeO₃ with A-site and B-site co-substitution....		82
3.1	Introduction	82
3.2	Experimental Procedure	82
3.3	Results and Discussion.....	84
3.3.1	Structural Studies.....	84
3.3.2	Activation Energy.....	91
3.3.3	Catalytic Behavior.....	94
3.4	Conclusion.....	98
CHAPTER 4: Influence of pH variation on the electrochemical properties of SrTiO₃.....		99
4.1	Introduction	99
4.2	Experimental Procedure	100
4.3	Results and Discussion.....	101
4.3.1	Structural Studies.....	101
4.3.2	Electrical and Impedance Studies.....	104
4.3.3	Electrochemical properties	112
4.3.4	FTIR Analysis	117
4.3.5	XPS Analysis.....	118
4.4	Conclusion.....	121
CHAPTER 5: Bifunctional catalytic behavior of La_{0.5}Sr_{0.5}Fe_{0.5}Ti_{0.5}O₃.....		122
5.1	Introduction	122
5.2	Experimental Procedure	122
5.3	Results and Discussion.....	124

5.3.1	Structural Analysis	124
5.3.2	OER/HER	126
5.3.3	Electrochemical irreversibility	129
5.3.4	Transient Response at interface	131
5.3.5	Stability Test.....	135
5.4	Conclusion.....	137
CHAPTER 6: Multifunctional HER/OER/ORR behavior with ZnO intercalation in LSFT ...		138
6.1	Introduction	138
6.2	Experimental Procedure	139
6.2.1	Target and base materials Preparation.....	139
6.2.2	Heterostructure Fabrication	140
6.2.3	Characterizations	140
6.3	Results and Discussion.....	141
6.3.1	Heterostructure formation and Conductivity	141
6.3.2	XPS Analysis.....	146
6.3.3	Bifunctional Behavior	147
6.3.4	Transient response at interface	150
6.3.5	Stability Test.....	153
6.4	Conclusion.....	155
CHAPTER 7: Effect of synthesis techniques on Sr doped Lanthanum Ferrite (LSF).....		156
7.1	Introduction	156
7.2	Experimental Procedure	156
7.3	Results and Discussion.....	157
7.3.1	Structural Studies.....	157
7.3.2	Surface Morphology and Particle Size	159
7.3.3	Electrochemical Analysis	161
7.4	Conclusion.....	165

CHAPTER 8: Conclusions and Future Scopes	166
8.1 Conclusion of the Present Investigation	166
8.2 Outlook for Future Perspective	170
References	172
List of Publications	184

LIST OF FIGURES

Figure.1.1 World energy consumption by different energy sources with projection from 2010 to 2030 [1].	2
Figure 1.2 Primary Global Energy Consumption 2023 [4]	3
Figure 1.3 Working of a Fuel Cell.....	8
Figure 1.4 Types of primary and secondary batteries.	11
Figure 1.5 Schematic illustration of water splitting.	14
Figure 1.6 Schematic of catalytic process at the electrode surface.	17
Figure 1.7 Reaction mechanism for Oxygen Evolution Reaction (OER) mechanisms in both alkaline (red) and acidic (blue) media[30].	19
Figure 1.8 Reaction mechanism for ORR.	21
Figure 1.9 Schematics of occurring reaction on bifunctional catalyst[31].	24
Figure 1.10 Structure of perovskite oxide.	26
Figure 1.11 Difference between the active site involved in pure electronic and mixed ionic electronic conductor.	31
Figure 1.12 Orthorhombic structure of LaFeO ₃ , Lanthanum is shown in green, Iron in gold and Oxygen in red.	44
Figure 2.1 Schematic of Solid-state reaction route.....	51
Figure 2.2 Schematics of Hydrothermal synthesis process.	52
Figure 2.3 PLD experimental set-up and schematics of Pulse laser deposition process.	53
Figure 2.4 The experimental setup of TGA/DSC.....	55
Figure 2.5 (a) Experimental setup of X-ray diffractometer [Rigaku Miniflex II, Japan] (b) Schematic representation of X-rays diffraction in a crystalline lattice.	57
Figure 2.6 (a) Mechanism and (b) experimental setup of Fourier transform infrared spectroscopy [JASCO 4600].	58

Figure 2.7 (a) Mechanism and (b) Experimental setup for the XPS spectroscopy (Kratos Amicus).	60
Figure 2.8 (a) Mechanism and (b) Experimental setup of SEM measurement [Nova Nano SEM 450].	61
Figure 2.9 Experimental setup of UV-Visible measurement [JASCO V-770 UV-Vis spectrophotometer].	63
Figure 2.10 (a) Mechanism (b) Experimental setup of TEM measurement [TECNAI G2 20 TWIN].	65
Figure 2.11 (a) Schematics of AFM (b) Experimental Set-up of AFM.....	67
Figure 2.12 Density measurement kit by Sartorius, BSA2245-CW.....	68
Figure 2.13 Experimental set up of automated impedance analyzer along with sample holder and furnace (a) 6500 P Wayne Kerr, UK (b) Solatron, SI 1260 Impedance analyzer, Ametek.	71
Figure 2.14 The equivalent circuit corresponds to the polycrystalline sample and their frequency response in the complex impedance plot.	74
Figure 2.15 Experimental set-up used for the electrochemical measurements (a) Keithley 2450 source meter (b) Multichannel Autolab PGSTAT – Metrohm with three electrode set-up.....	76
Figure 2.16 Current-potential curve of a CV measurement	77
Figure 2.17 Current-potential curve of a LSV measurement.	78
Figure 2.18 Representative image of structural refinement fit of XRD data using FullProf Suite of the LaFeO_3	81
Figure 3.1 XRD pattern of the sintered LF, LSF, LSFT.	84
Figure 3.2 Rietveld refinement of XRD pattern for LF, LSF, and LSFT.....	85
Figure 3.3 (a) Change in the orientation of BO_6 octahedra with a substitution for LF, LSF, and LSFT (b) SEM micrographs with the change in morphology.....	87
Figure 3.4 (a) Diffuseness of the highest intense peak corresponding to $2\theta \sim 32^\circ$ for LF, LSF, and LSFT (b) corresponding unit cell crystal structure shown with distortion of FeO_6 octahedra for LaFeO_3 (c) Variation of conductivity with temperature (d) Octahedral splitting with vacant d-orbital for LF, LSF, and LSFT.....	88
Figure 3.5 (a) Tauc plot for band gap estimation, in inset variation of absorbance with wavelength..	89

Figure 3.6 Electron density plot in the x-y plane for LF,LSF, and LSFT at room temperature.	91
Figure 3.7 (a)–(c) Arrhenius plot ($\ln \sigma$ vs $1000/T$) with linear fitting in low temperature (LTR) and high temperature regimes (HTR) for LF, LSF, and LSFT and (d) activation energy for LF, LSF, and LSFT.	92
Figure 3.8 Variation of mass with temperature of the studied samples LF, LSF, and LSFT.	93
Figure 3.9 (a) Third quadrant of CV curves showing the maximum ORR in LSF (CV curve at the scan rate of 50 mV/s) (b) Charge Transfer Coefficient with bandgap for LF, LSF, and LSFT (c) Charge carrier distribution over the active site for a span of 4000 s using the Finite Element Simulation technique, C_{surf} is the concentration of species at surface.	94
Figure 3.10 Shoup-Szabo fitting of the studied samples LF, LSF, and LSFT.	96
Figure 3.11 R-S equation fitting of the studied samples LF, LSF, and LSFT.	97
Figure 3.12 Tafel Slope of the studied samples LF, LSF, and LSFT.	97
Figure 4.1 (a) Powder X-ray Diffraction of sintered SrTiO ₃ sample with JCPDS (350734) (b) Rietveld refinement of SrTiO ₃ (c) W–H plot of SrTiO ₃ (d) TGA curve of weight loss and the mass change with temperature SrTiO ₃	102
Figure 4.2 Inset shows the zoomed -in version of SEM micrograph of the sintered pellet and particle size calculation histogram.	104
Figure 4.3 (a) Variation of $\log \sigma$ vs $\log v$ at various temperatures (b) $\log \sigma_{dc}$ vs $\log v_h$ (c) $\log \sigma_{dc}$ vs $1000/T$ (d) $\log v_h$ vs $1000/T$ for activation energy (e) variation of exponent with temperature and (f) charge carrier concentration with temperature.	105
Figure 4.4 (a) Nyquist Plot from 400 °C to 575 °C (b) at low temperature (50 °C to 375 °C) (c) at high temperatures (600 °C to 700 °C) imaginary part of Z vs real component of Z.	107
Figure 4.5 Frequency dependence of (a) real part of Z (b) imaginary part of Z (c) modulus of Z (d) Nyquist plot with the equivalent circuit at 500 °C.	109
Figure 4.6 Ghosh scaling of SrTiO ₃	110
Figure 4.7 (a) Electric modulus spectra of SrTiO ₃ at various temperature (b) frequency variation of Electric Modulus M''/M''_{max} and impedance Z''/Z''_{max} at 350 °C.	111

Figure 4.8 Cyclic voltammograms of SrTiO ₃ at (a) neutral (b) basic (c) acidic medium and peaks of oxidation and reduction in (a.1) neutral medium (b.1) basic medium.....	112
Figure 4.9 (a) First and second derivative at the scan rate 100 mV/sec (b) $E_{p/2}$ and E_i with the scan rate.....	114
Figure 4.10 Variation of (a) $\log j$ vs $\log v$ (b) current density with scan rate $v^{1/2}$	115
Figure 4.11 Current-time response at 2V (a) neutral medium (b) basic medium.....	116
Figure 4.12 FTIR spectra of SrTiO ₃	117
Figure 4.13 X-ray photoelectron spectroscopy measurements (de-convoluted peaks) of SrTiO ₃ (a) the wide spectra (b) O1s spectra (c) Sr3d spectra (d) Ti2p spectra.....	119
Figure 5.1 (a) XRD with Rietveld refinement of LSFT (b) Tauc plot to estimate band gap, inset shows the absorbance curve obtained from UV-Visible spectrophotometer, (c) depicts the y-z plane of the LSFT structure. (d) Band structure showing conduction band minimum (CBM) lies at 1 eV while valence band maximum (VBM) lies at -0.75 eV, (e) depicts the active surface containing Fe,Ti and O where (d-metal ligand) ORR occurs whereas OER takes place with the formation of passive layer containing La site.....	125
Figure 5.2 Valence band maximum (VBM) determination using X-ray photoelectron spectroscopy.....	126
Figure 5.3 Cyclic voltammograms with the variation of scan rate and pH.....	127
Figure 5.4 (a) Cyclic voltammograms with the variation of pH at 10 mV/sec scan rate, inset (i) Cyclic voltammogram at pH =1, inset (ii) Cyclic voltammogram at pH =14 (b) variation of HOMO and LUMO states with pH (b) inset variation of difference of HOMO and LUMO states (ΔE) with pH.....	128
Figure 5.5 (a) R-S equation plot between the current density and v with pH variation (b) log-log plot of current density and v with pH variation.....	129
Figure 5.6 Current density, first- and second-order derivative CV curves at 10 mV/sec for the estimation of the parameters $E_{p/2}$ and E_i with the variation of scan rate and pH.....	130
Figure 5.7 $E_{p/2}$ and E_i , estimated from the first- and second-order derivative of forward scans of CV curves (Fig 5.3) are with the scan rate for pH variation.....	131

Figure 5.8 Chronoamperometric curve of current density and time with pH variation.....	132
Figure 5.9 Shoup-Szabo fitting with pH variation.	133
Figure 5.10 Mott Schottky fitting with pH variation suggesting n-type behavior in pH =1 and 14 while p-type behavior is observed in pH=7.....	134
Figure 5.11 Cycle Stability of LSFT for 600 cycles in neutral media (pH =7).....	136
Figure 5.12 (a) Stability for LSFT up to 1500 h in neutral media (pH =7) with cell potential of 2V for current 150 mA/cm ² (b) Current density and potential plot over a range of 1500 h.	136
Figure 5.13 Chronopotentiometric stability of 1500 h as compared to other neutral pH bifunctional catalysts.	137
Figure 6.1 (a) Heterostructure preparation i.e., intercalation of ZnO between LSFT, (b) SEM micrographs for $n = 10$ illustrating the thickness of ZnO layer, (c) X-ray diffraction patterns of DH-MIECs and presence of peaks (d) Variation dc conductivity with temperature , inset shows the relative conductivity of DH-MIECs with respect to $n=0$ (e) Current density (j) vs electric field (E) curve.	143
Figure 6.2 (a) Mix ionic electronic behavior for the parent sample along with the DH-MIECs (variation of I/I_0 vs. time) using coulometric method (b) Activation energy plotted with the n variation, inset shows the difference of activation energies from Arrhenius and nearest neighbor hopping plots of conductivity.	144
Figure 6.3 (a) Variation of transmittance for $n = 10$ and $n = 15$ DH-MIECs, arrows are showing the characteristic peaks corresponding to Fe-O, La-O, Ti-O, Sr-O and Zn-O, (b) Surface topographical images from AFM indicating larger grain size and smaller roughness for $n = 15$	145
Figure 6.4 Deconvoluted XPS spectra corresponding to O, blue colored peak corresponds to metal-O bond, black colored peak corresponds to metal-OH bond and light orange colored peak corresponds to Auger electrons.	147
Figure 6.5 Cyclic voltammograms of different DH- MIECs with the variation of scan rate.	148
Figure 6.6 Linear sweep voltametric (LSV) curves in (a) HER, (b) OER and (c) ORR regimes and a comparative is prepared with Pt working electrode.....	149
Figure 6.7 (a) RS equation plot between the current density and scan rate, ν and (b) log-log plot of current density and ν of all DH-MIEC with parent LSFT.....	150

Figure 6.8 Chronoamperometric response of all DH-MIECs with parent LSFT.	151
Figure 6.9 Shoup-Szabo fitting of all DH-MIECs with parent LSFT ($n = 0$).	152
Figure 6.10 Mott Schottky fitting with pH variation suggesting n-type behavior in pH =1 and 14 while p-type behavior is observed in pH=7.....	153
Figure 6.11 (a) Chronopotentiometric stability in OER regime for 25 h resulting in the potential of 1.66 V for $n = 15$ (b) Variation of transmittance from IR spectra, inset shows the surface topographical images before and after stability test for $n = 10$ and $n = 15$ DH-MIECs (c) Deconvoluted O XPS spectra before and after stability test for $n = 15$ DH-MIEC.	154
Figure 7.1 (a) X-ray diffraction patterns of B-LSF and N-LSF (b) Reitveld refinement of both B-LSF and N-LSF.	158
Figure 7.2 W-H plot of of B-LSF and N-LSF and estimated value of micro strain.	159
Figure 7.3 (a)-(b) SEM micrograph of Bulk LSF and Nano LSF particles.....	160
Figure 7.4 (a) TEM images of Nano-LSF confirms the formation of nanoparticle (b) TEM micrographs with particle size distribution (c) SAED pattern.....	161
Figure 7.5 Cyclic Voltammogram curve of (a) B-LSF (b) N-LSF with various scan rate.....	162
Figure 7.6 Specific capacitance at different scan rate for B-LSF and N-LSF sample.....	163
Figure 7.7 Specific capacitance at different scan rate for B-LSF and N-LSF sample.....	164
Figure 7.8 Variation of current density with $v^{1/2}$ in (a-b) and (c-d) are log-log plot of current density and v	164

LIST OF TABLES

Table 1.1 Different types of fuel cells with their characteristics.	10
Table 1.2 Structural Predictions for the Goldschmidt tolerance factor	27
Table 1.3 List of well-known perovskites.....	28
Table 1.4 Applications of frequently studied perovskites	29
Table 1.5 List of Fe-based perovskites and their properties.	37
Table 1.6 Summary of cyclic stability of previously investigated perovskites.	43
Table 2.1 Description of the raw materials with their chemical formula, purity, and manufacturer used for the preparation of proposed compositions.....	49
Table 2.2 All detailed relations of complex quantities[153].....	72
Table 3.1 Structural Parameters of sample at 300 K	86
Table 3.2 Bond lengths and angles at 300 K	90
Table 4.1 Parameters obtained from the refinement.....	103
Table 5.1 Electrochemical parameters of samples at 300 K.....	134

LIST OF SYMBOLS AND ABBREVIATIONS

FC	Fuel Cell
SOFC	Solid Oxide Fuel Cell
PEMEC	Proton Exchange Membrane Fuel Cell
AFC	Alkaline Fuel Cell
PAFC	Phosphoric Acid Fuel Cell
MCFC	Molten Carbonate Fuel Cell
DMFC	Direct Methonal
OER	Oxygen Evolution Reaction
ORR	Oxygen Reduction Reaction
HER	Hydrogen Evolution Reaction
CV	Cyclic Voltammetry
LSV	Linear Sweep Voltammetry
LF	Lanthanum Ferrite
LSF	Lanthanum Strontium Ferrite
LSFT	Lanthanum Strontium Ferrite Titanate
ST	Strontium Tiatanate
DH-MIEC	Double Heterostructure Mixed-Ionic Electronic condcutor
VB	Valance Band
CB	Conduction Band
eV	Electron Volt
meV	Milli-electron Volt
E_g	Band Gap
E_a	Activation Energy
$h\nu$	Photon Energy
k_B	Boltzmann's constant
FWHM	Full Width at Half Maximum

g	Gram
K	Kelvin
T	Temperature
ICDD	International Center for Diffraction Data
JCPDS	Joint Committee on Powder Diffraction Standards
M, M', M''	Modulus, real and imaginary modulus
Z, Z', Z''	Complex, real and imaginary impedance
σ	Conductivity
τ	Relaxation time
ω	Angular frequency ($2\pi f$)
η	Exponent
θ	Diffraction angle
RT	Room Temperature
Å	Angstrom
mg	Milligram
N	Avogadro's Number
nm	Nanometer
cm	Centimetre
μm	Micro-meter
Pt	Platinum
mV	Milli Volt
hz	Hertz
Ag	Silver
SEM	Scanning Electron Microscope
TEM	Transmission Electron Microscopy
XPS	X-Ray Photoelectron Spectroscopy
UV-Vis	Ultraviolet-Visible
DSC	Differential Scanning Calorimetric
PLD	Pulse Laser Deposition

CPE	Constant Phase Element
XRD	X-ray Diffraction
TGA	Thermogravometric Analysis
SSR	Solid State Reaction
F	Faraday's Constant
n	Number of electrons
v	Scan rate
RHE	Reference Hydrogen Electrode
V	Voltage/Potential
HOMO	Highest Occupied Molecular Orbital
LUMO	Lowest Unoccupied Molecular Orbital